EFDA–JET–PR(09)37

A. Quercia, R. Fresa and JET EFDA contributors

The New Ex-Vessel Magnetic Measurements in JET: A Critical Assessment of the Collar Probe

The New Ex-Vessel Magnetic Measurements in JET: A Critical Assessment of the Collar Probe

A. Quercia[1,2], R. Fresa[1,3] and JET EFDA contributors*

JET-EFDA, Culham Science Centre, OX14 3DB, Abingdon, UK

[1]Consorzio CREATE - Associazione EURATOM-ENEA, Via Claudio 21, I-80125 Napoli, Italy
[2]Dipartimento di Ingegneria Elettrica, Universitá degli Studi di Napoli Federico II
[3]Dipartimento di Ingegneria e Fisica dell'Ambiente, Universitá degli Studi della Basilicata
** See annex of F. Romanelli et al, "Overview of JET Results",*
(Proc. 22 [nd] IAEA Fusion Energy Conference, Geneva, Switzerland (2008)).

Preprint of Paper to be submitted for publication in
Fusion Engineering and Design

ABSTRACT.

The paper deals with a new set of magnetic probes which has recently installed in JET in order to improve the field measurements in the proximity of the iron. The set consists of six Limb probes, attached to the upper horizontal iron yokes, and one Collar Probe, inserted in the collar region of the iron structure. The probes include pick-up coils, flux loops, Hall sensors, and a temperature sensor.

The data provided by the system are regularly acquired and recorded within the set of JET Pulse Files. They are ready for use in studies implyingmeasurement of the stray field due to the residualmagnetization, as well as for all the modeling activities involving 3D studies, in particular resistive wall mode studies, more accurate modeling for the vertical stabilization, interactions between NBI and magnetic field. In addition, the experience gained with Hall transducers is considered valuable in view of their potential use in ITER.

Unlike the limb probes, the collar probe did not pass the functional commissioning, due to an unexpected discrepancy between the signals from Hall sensors and pick-up coils. The analysis illustrated in the paper shows how a critical assessment of the local configuration and a suitable magnetic modeling could solve this commissioning issue. In the case of the collar probe, it is demonstrated that the measurements are acceptable, since the observed discrepancy is due to a local geometrical effect, which was not known at the time of the installation.

The paper also includes some other more general information, which might be useful for JET studies.

1. INTRODUCTION

The Ex Vessel Probe (EVP) system [1–7] was installed during the 2005 shutdown as part of the JET-EP Enhanced Performance programme [8] and made available for use in the 2006 and subsequent JET experimental campaigns. It consists of a set of Hall, pick-up coils and flux loops sensors. The main aims of the system are:

- provide experimental data for better modeling the characteristic of the iron in the axisymmetric codes for plasma equilibrium reconstruction
- test the reliability of Hall sensors in presence of neutrons
- use the *absolute* field measurements obtained from Hall sensors to correct the drifts/offsets of the integrators.

The voltage signals produced by the inductive sensors (pickup coils and flux loops) represent the time-derivative of the physical quantity to be measured, the magnetic flux density, B (spatially averaged, as discussed in Section 2).[1] Hence, these signals need to be integrated in time, and that is conveniently done by analog integration.[2] The integration constant (the field B_0 at the initial instant) is not known, and so the inductive transducers cannot provide an *absolute* measure of the field, but

[1] *The article includes some other more general information which, thanks also to the references, might be useful for JET studies.*

[2] *To integrate and acquire an analog signal into digital form there are two possibilities: a) Analog Integration + Analog to Digital Conversion (ADC); b) ADC + Digital Integration. Option a) is generally preferred, since a dB/dt signal is tipically a continuous sequence of spikes, difficult to correctly (and/or optimally) convert into digital form. However, the adoption of advanced techniques could make option b) viable too.*

only a *relative* one. $\boldsymbol{B}_0$ is fictitiously fixed to zero within the integration process. In the case of JET, the initial field is mainly related to the residual magnetization of the iron core and to the current (± few hundreds kA) flowing in the primary circuit (Fig.9) before the start of each pulse.

The Hall sensors give an *absolute measure*, so they can provide the steady state value $\boldsymbol{B}_0$.

Another issue is related to the *input offset* of the operational amplifiers constituting the integrators, which reflects in a drift on their outputs. This drift can be corrected by comparing the relative measures provided by the inductive sensors with the absolute output of the Hall sensors.

The ability to provide a drift correction is crucial for ITERlike devices, where long lasting flat-top phases are expected, in an high neutron yield and high temperature environment [9].

In JET, the probes are located very near to the iron structure, in the proximity of the upper horizontal iron yokes 3-4 and 8-1 and in the iron collar region at Octant 4, so to provide useful information for the tuning of the code parameters representing the characteristics of the iron.

The data provided by the EVP system are ready for use in studies implyingmeasurement of the stray field due to the residual magnetization, as well as for all the modelling activities involving 3D studies, in particular resistive wall mode studies, more accurate modelling for the vertical stabilization (at the moment only approximate 2D models are available), interac-tions between NBI and magnetic field.

As a conclusion of a first phase of the commissioning of the EVP system, completed in 2006, all sensors provide useful signals, which are regularly stored in CODAS (Control & Data Acquisition Systems) and included in the set of JPF (JET Pulse Files).

A second phase of the commissioning process then started (*functional commissioning*), aimed at assessing the physical meaning of the recordedmeasurements. As a conclusion of this second phase, only the signals produced by limb sensors were found to provide the expected field values and are then scientifically exploitable, whereas the use of the Collar Probe for the above mentioned applications appears to be questionable. In fact, in spite of the fact that the sensors measure the field correctly, values are strongly affected by the local geometry of the iron, which is responsible for a remarkable spatial gradient. This conclusion is supported by the analysis described in the paper. The bulk of the paper is then dedicated to a critical assessment of the signals produced by the sensors in the collar region.

2. DESCRIPTION OF THE EVP SUBSYSTEM

Figure 1 shows the toroidal location of the sensors. The system consists of three subsystems, with 7 probes in total:

- Limb Probe 3-4 subsystem: 3 probes attached to the upper horizontal iron yoke 3-4, in blue
- Limb Probe 8-1 subsystem: 3 probes attached to the upper horizontal iron yoke 8-1, in dashed blue
- Collar Probe subsystem: one probe inserted in the collar region of the iron structure at Octant 4, in pink.

Each Limb Probe subsystem is composed of an Inner, a Centre and an Outer probe. In turn, each of the 6 limb probes includes the following three types of magnetic sensors:

a) 1 Hall sensor, which measures the z (vertical) component of the magnetic flux density, B_z
b) 1 pick-up coil, which measures the variation of the z component of the magnetic flux density, $d/dt\ B_z$
c) 1 (local) flux-loop, which measures the variation of the spatial average of the z component of the magnetic flux density over the open surface S bounded by the winding, $d/dt\ \langle B_z \rangle s$ [5].

The flux-loops are not to be confused with *full* flux-loops, namely they do not measure the poloidal flux ψ. As schematically represented in Fig.1, they are large coils local to the iron yokes they are anchored to. In limb 3-4 their toroidal span is 45 degrees, whereas on limb 8-1 they occupy toroidally the dimension of the iron yoke [4, 6].

Strictly speaking, the signals produced by a pick-up coil is more correctly identified as measuring the variation of the spatial average of the relevant component of the magnetic flux density over the volume occupied by the winding, $d/dt\ \langle B_{r,z} \rangle_\tau$. This remark is usually not important because, due to the relatively small size of the coils, the field can almost always be considered uniform in the volume τ. This is not the case of the Collar Probe (as it will be shown), which includes:

i) 2 Hall sensors, measuring the r (radial) and z components of the magnetic flux density, $[B_r\ B_z]$
ii) 2 pick-up coils, measuring the variation of the spatial average of the r and z components of the magnetic flux density over the volumes r and z occupied by the windings, $d/dt\ [\langle B_r \rangle_{\tau_r}\ \langle B_z \rangle_{\tau_z}]$
iii) 1 temperature sensor.

There are in total 22 magnetic sensors and 1 temperature sensor.

The voltage signals produced by the pick-up coils and by the flux-loops are analog-integrated in the front-end of the data acquisition cards in the CODAS cubicle.

A complete description of the system, the installation and commissioning activities/issues, including open points and other informative material, can be found in [4].

The EVP signals are listed in Table 1. The previous issue of this table [10] labelled the signals produced by limb sensors as reliable and the ones produced by the collar sensors as non reliable, meaning that it was recommended to include in the public PPF (Processed Pulse Files) the limb signals only. The reason was that the information contained in the collar signals was not yet properly understood. As an outcome of the analysis shown in this paper, the collar signals are now considered reliable.

3. CRITICAL ASSESSMENT OF THE COLLAR PROBE MEASUREMENTS

3.1. THE COLLAR PROBE ISSUE

Figure 2 shows the cross-section configuration of the JET machine [11], with a schematic representation of the location of the Collar Probe (red dot) added. Crucial mechanical components, described later, are not shown here. Figure 3 depicts the Collar Probe, in terms of CAD models and finalised system. The coils measure (after analog integration) the average value of the magnetic

flux density B in the volume occupied by the winding, whereas the Hall sensors measure *local* values of B. The centres of the r and z pick-up coils are coincident. The distances between the 2 Hall sensors and the centre of the coils are circa 3.1cm and 3.5cm [4]. The *Collar Probe issue* consists then in the fact that the signals produced by the coils are significantly different from the signals produced by the Hall sensors, as described below and in the commissioning report [4].

3.2. PRELIMINARY ANALYSIS

The measurements produced by the Collar sensors are well reproducible but, as stated, they don't seem to be physically consistent. In particular, the signals produced by the 2 pickup coils (ECC4R for the radial component and ECC4V for the vertical component) are different from those produced by the 2 Hall sensors (EHC4R and EHC4V respectively) by almost 20% and up to 40mT in absolute terms [4]. Such a large discrepancy of measurements exists also in absence of toroidal field currents. Being the Hall sensors and the pick-up coils located just about 3 cm apart, the local nonuniformity of the field was initially considered not sufficient to justify the discrepancy.

Several working hypotheses were put forward to explain this behaviour, such as swapping of cables, misalignment of sensors and erroneous calibration constants. None of them appeared to provide a coherent interpretation of the measurements in all the cases considered [4]. Effects due to the operating temperature of the Hall sensors were also ruled out, because the Pt1000 sensor built in the probe indicates that the temperature does not exceed 30–35C.

Many hardware tests were performed in order to verify the Collar equipment, but no evidence of any clear shortcoming in the sensors, in the cabling and in the signal conditioning electronics in the CODAS cubicle emerged [13, 14].

It seemed then necessary to uninstall the system from the machine for a complete bench test and calibration, and/or to develop an accurate 3D model of the collar region in order to quantitatively estimate the grade of local non-uniformity of the field due to the many holes present in the torsion collar component [15].

The function of the holes present in the Torsion Collar was not completely clear, hence it was decided to make a preliminary assessment of all the components present in the collar region, with the aid of various generations of the JET assembly, detail and configuration drawings [16]. The outcome of this assessment was reported in [17].

3.3. ASSESSMENT OF THE LOCAL CONFIGURATION

Figure 4 shows the Torsion Collar component. As outlined in the caption, the documentation used during the design phase of the collar probe was not complete. In particular, the CAD model of the torsion collar component seems to be based on the original JET drawing D730-01-001 (collar segment casting) which does not show the through hole where the collar probe is effectively inserted. The function of the 3 larger holes in the torsion collar was not properly understood.

The torsion collar is ferromagnetic and was designed to be so in order to direct the magnetising flux into the inside of P1 polidal solenoid. Originally the P1 solenoid was shorter [11, 12] and

matched the geometry of the magnetic ring more closely than it does now. With P1 now longer (made of 10 coils, Fig 2), the collar is probably less efficient, but could not be easily changed [18].

The complete torsion collar is made of 8 parts (one per Octant) mutually isolated [19–21], so that the circulation of axisymmetric eddy currents is prevented. However, each of the 8 parts is a bulky, highly conductive object (with resistivity at 20C, ρ_{20} = 2.28E-6Ωm [22], just about double than in-conel®600) and so, given its dimensions (for instance radial dimension is 1040mm), a time constant of the order of 1 s is estimated. However, the simulations shown in the next sections are magnetostatic, i.e. eddy currents are neglected. This is not critical for our present purposes, and will be reconsidered in a future work.

Figure 5 gives an overview of selected parts of the JET mechanical structure, showing in particular the Collar Teeth components. In (a) the lower side is shown, including ring, collar and inner cylinder. In the middle of two consecutive toroidal field coils, in each of the two collar regions (upper and lower), there is a collar tooth. (b) is part of the original JET drawing D730-01-001 (mechanical structure general assembly); the upper and lower collar teeth are circled. In (c) there is a particular of the collar region from the *unpublished* JET drawing FN338 117. We see that, other than the collar teeth (circled in red), there are also the larger *ring teeth* (circled in blue) holding the toroidal field coils. The design team of the collar probe was aware of the presence of teeth holding the toroidal field coils, in particular the presence of the ring teeth was known. (d) is the CAD model of the collar region with the collar probe positioned; the ring teeth are visible on the right, whereas the collar teeth are missing.

The collar and ring teeth help the toroidal field coil set to withstand the up-down antisymmetric electromechanical torques due to the presence of the (mainly vertical) poloidal field [23–26].

A representation of the relevant poloidal section in the collar region is reported in Fig.6. The central collar tooth is very close to the sensors, circa 5cm, so the magnetic field can significantly vary in the volume occupied by the sensors. The sensors are represented by small dots, which for the coils indicate just the centre of the windings. The direct contribute to the local field from far sources (plasma, active and passive conductors) is shielded by local effects. Due to the geometry of the tooth, a point/edge effect is foreseeable in the field map.

The materials of the JET magnetic circuit (Fig.7) and mechanical structure are listed in Table 2.

3.4. EFFECTS OF THE MAGNETIC PROPERTIES OF THE MATERIALS

A set of seven *H-B* curves is historically available in the form of lookup tables for the various parts of the magnetic circuit of the JET machine [22, 27] (the characteristic of the Collar Teeth is not included in the set). The original plots for some of the components (Centre Pillar, Centre Pieces and Limbs, PF1 Support Rings, and Torsion Collar) are available online [28]. Although the various materials are different, most JET codes use only one *non-hysteretic H-B* characteristic (the same curve for all the materials). The first version of Proteus, which was installed at JET in late 80's used a single curve as well (Fig.8), which was the same as the SCED code and probably the same as the present JET version of Proteus [27, 28]. The above curve is also used by many modern codes of

current use at JET (including the one we used to perform the simulations described in the next sections).

For the majority of purposes, the actual *H-B* curve is not that important, because:

- The iron in the Central Column is fully saturated whenever the m.m.f. $|NI|$ is above a relatively low threshold NI_{TH}. In terms of the current I_{PRIM}, flowing in the *primary circuit* (Fig.9), $I_{PRIM,TH}$ is few hundreds Amperes
- It happens to be $|NI| < NI_{TH}$ generally only[3] at the beginning of JET pulses (both in *Mode B* and *Mode D* [29]), when there is the inversion of the I_{PRIM} current, and anyway during this relatively small interval the control is not critical[4]
- The iron of the Limbs is always far from saturation (and so $H \cong 0$ in the Limbs)
- The only region where the *H-B* curve plays a role is the Torsion Collar (the polar shoe) i.e. where the cross-section of the iron nearly doubles with respect to the part inside the P1 coil.

In our case, we want to make an assessment of the Collar Probe by simulating the magnetic flux density at locations very close to specificmagnetic components. Hence the effective *H-B* curves may play a role. However, the curve of Fig.8 is quantitatively very close to the curve of the Torsion Collar, and to the one of the Centre Pillar, Centre Pieces and Limbs as well.

Regarding the magnetic behaviour of the collar teeth, its determination is relatively straightforward. In fact, when the carbon content of an annealed carbon steel is n*low* (tipically around 1% and below), the main parameters of its *hysteretic H-B* diagram mainly depend on the carbon content itself [31–35]. Namely, the saturation magnetization M_S, the coercitive force H_C and the maximum relative permeability μ_{rm} are plotted versus the carbon content [31]. The material of the collar teeth is indeed a 0.38% carbon steel, so its parameters (already listed above) are easily determined. An hysteretic piecewise linear approximation is then defined by the equations $B = \mu_0\mu_{rm}(H \mp H_c)$ for the lateral segments, $B = \mu_0(H \pm M_s)$ for the saturation half-lines, and the knees are at $(H_k^{up}, B_k^{up}) = \frac{\mu_{rm}}{\mu_{rm}-1}\left(\frac{M_S}{\mu_{rm}} - H_c, \mu_0(M_s - H_c)\right)$, $(H_k^{low}, B_k^{low}) = -(H_k^{up}, B_k^{up})$. The sought non-hysteretic case follows for $H_c = 0$: $H_k = 840$A/m ($\mu_0 H_k = 1.05$mT), $B_k = 2.11$T.

[3] *It is worth to remember that actually it regularly results to be* $|NI| < NI_{TH}$ *during the* end of pulse sequence *as well. In fact, after the end of each pulse, the* I_{PRIM} *current is reset to a negative value of few hundreds Amps, and that is the reason why, before the start of every pulse, the steady state field measured by the Hall sensors is always about the same. Another consequence is that it's not so straightforward to measure the hysteresis curve of the JET magnetic circuit.*

[4] *Recently there is a renewed interest in studying the* breakdown *phase (when plasma is born at the beginning of each pulse), with the aim of reducing the number of conditioning dry runs and unsuccessful pulses in general. At the moment the breakdown is implemented by using a simple recipe (adapted depending on the turn option used for the PF coils [30]) which tries to keep the null in the centre of the chamber during the rise of* I_{PRIM}*. The idea is to introduce feedback control for the breakdown in order to get enhanced results. In a mode D pulse [29], plasma is born during the fast rise of* I_{PRIM}*, before* I_{PRIM} *itself reaches the hysteretic zone. In mode B that is actually not exactly the case, but anyway we believe there is still no issue in using the single curve of Fig.8. 3D effect are thought to be eventually more important in this respect, rather than the properties of single elements of the magnetic circuit.*

In the next sections we show some results of a preliminary magnetostatic modeling activity. We did not implement the piecewise linear approximation for the collar teeth or a smoother version of it, we used the curve of Fig.8 for all the materials instead. In a future work, a more accurate sensitivity analysis will be done, a refined and optimized mesh will be included in the model, and the effect of eddy currents circulating in the passive structures will be taken into account [36–38].

3.5. ANALYSIS OF THE SIGNALS FROM THE COLLAR SENSORS

In order to assure reproducibility, and to get statistical significance, a number of JET pulses were considered for the analysis. In particular, waveforms for the standard dry run 64444 are represented in Fig.10. The first two plots depict the currents in the Poloidal Field (PF) *circuits* [39] and in the Toroidal Field (TF) coils, which give power to the machine. Third plot shows the *raw* signals produced by the magnetic sensors of the collar probe. In the last plot, the same signals are *linearly* TF compensated[5] with reference to values in the interval 38.0-39.8s [40]. The TF currents rise approximately in the interval 26-36s, but it is apparent, in the EHC4R signal, a nonlinear/saturation-like effect starting at t = 29s; that is due to the fact that the collar teeth and the sensors are located between two adjacent TF coils and they are very close to each other, and the (3D) field produced by the TF currents rapidly grows in that region. Moreover, even in the case of the pulse here considered, where there is no extra ripple,[5] *toroidal ripple* (the poloidal field generated by the TF currents) is present anyway, making the analysis more involved. When the *I*P4T current rise, the correspondent poloidal field probably acts on the ferromagnetic teeth, modifying the orientation of their magnetic domains. Nonlinear and 3D effects are hence particularly significant, and the standard *linear* TF compensation technique is only considered here in order to show the involved issues.

The sensors do not respond to the rise of I_{PRIM} and very minimally respond to I_{PFX}. That is not unexpected. In fact the primary circuit (Fig 9) is specifically designed in order to produce flux but not to produce field in the vacuum vessel, in particular to eliminate the stray field before plasma breakdown [23]. To that purpose, a major role in JET is played by the iron. And then, thanks to the fact that the primary circuit also implies circulation of the current in few turns of the P3 coils (2 turns in P3U and 2 in P3L) [39], a null is created in the centre of the vessel. This kind of configuration is more important in machines without magnetic circuit.

[5] *The considered signals are produced by sensors which are obviously not perfectly built and are not perfectly aligned along the design direction. Thus for instance, the sensor ECC4R is designed to measure the B_r component of the field but, being its magnetic axis not exactly oriented along the radial direction, the signal it produces contains some amount of pick-up from the B_z and B_ϕ components. If the unit-vector $\hat{\boldsymbol{n}}$ specifies the orientation of the magnetic axis, and $(\alpha, \beta, \gamma) = (\hat{\boldsymbol{r}} \cdot \hat{\boldsymbol{n}}, \hat{\boldsymbol{z}} \cdot \hat{\boldsymbol{n}}, \hat{\boldsymbol{\phi}} \cdot \hat{\boldsymbol{n}})$ are its direction cosines, it is $B_{ECC4R} = \alpha B_r + \beta B_z + \gamma B_\phi$, with $\alpha \cong 1$, $|\beta| << 1$, $|\gamma| << 1$. In particular, the toroidal field is stronger than the poloidal one, giving $B_{ECC4R} \cong B_r + \gamma B_\phi$, and the necessity of correcting the signals produced by the sensors of the aliquot of the toroidal pick-up. Assuming linearity, gives $B_{ECC4R} = B_r + c_{odd} I_{TFodd} + c_{even} I_{TFeven}$, so to extract B_r it is sufficient to determine the constants codd and ceven, which can be done by considering a dry run, and specifically instants (better averaging over intervals) when $B_r = 0$, namely when the TF currents only are nonzero [40]. For the sensors of the JET machine it is probably always possible to assume linearity, exept in this specific case of the Collar Probe; we consider it here for illustrative purposes.*

[6] *Except when performing ripple experiments, the odd end even TF coil sets are connected in series, thus $I_{TFodd} = I_{TFeven} = I_{TF}$.*

The instant $t = 48.5$s is considered for the simulations described in the next sections, where only the I_{PRIM}, I_{P4T} and TF currents are nonzero.

3.6. 2D FEM MODELING

Figure 11 shows axisymmetic flux maps for the standard dry run Pulse No: 64444 at $t = 48.5$s. Only I_{PRIM}, I_{P4T} and TF currents are nonzero. The *H-B* curve of Fig.8 is used for all the materials. Three different local geometries were considered: (a) and (b) respectively refer to magnetostatic simulations without and with axisymmetric collar tooth, whereas in (c) an axisymmetric through hole in the torsion collar (where the support of the collar probe is inserted) is added too.

In (b) we see that the collar tooth introduces significant local effects, and in (c) the hole (in this axisymmetric simulation) further modifies the local field at the locations of the collar sensors. The values of the simulated field inside the through hole are not meaningful, because in reality the through hole is not axisymmetric but cylindrical, and the field is expected to vanish inside. The complete flux map for the third case is given in (d).

Table 3 lists result and comparisons of themagnetostatic simulations and the experimental values for the sensors in the Upper Collar region at $t = 48.5$s of the standard dry run Pulse No: 64444. The introduction of the axisymmetric tooth greatly alters the components of the simulated fields at the locations of the sensors (50 to 80%, line b – a), and the through hole further modifies the values (19% on the Hall vertical component, line c – b). The differences between the simulated fields seen by the Halls and the coils become significant as well (last two columns), in analogy to what the experimental signals show (line e). Actually, comparing the values in the last two columns of lines c and e we see opposite signs of $\Delta B_r\%$ and $\Delta B_z\%$; that does not mean that those results are incompatible, in fact to make a proper comparison in this case we should think in terms of amplitude and angle, rather than in terms of field components. An extensive comparison between the simulated and the experimental signals appears to be not appropriate at this stage, due to the combined effects of the 3D geometry, the strong toroidal field and ripple, and peculiar nonlinear complexities. In this preliminary analysis, to simulate the signals of the pickup coils, the field in the centre of the coils is considered. Gaussian quadrature should be employed for a more accurate evaluation.

3.7. 3D FEM MODELING

As seen, in the region occupied by the collar probe there are a number of local phenomenon, in particular a significant spatial gradient and peculiar nonlinear effects. Moreover, the added poloidal field induced by the TF currents is always present (even in pulses without extra TF ripple), and the eddy currents may possibly play a role as well.

In order to increase the confidence, a 3D modeling activity is being carried out.

A first mesh (Fig 12 (a)-(c)), consisting of 26052 brick elements, 42963 nodes and 94687 faces, was built and integrated with the CARIDDI code [36–38], which implements an iterative procedure based on an integral formulation. That implies circa 30000 unknowns and 3.5GB of RAM in single precision, for the *L* matrix only. The model includes magnetic circuit, vacuum vessel and divertor,

whereas the mechanical structure is omitted. Due to the symmetries, it is sufficient to model 22.5 degrees (1/16) toroidally. For each of the 7 types of iron, the proper permeability curve description [22, 27] is used. However, this is not expected to give important changes in general (see what said for Fig.8). The magnetic behaviour of the teeth is implemented as well. The material of the dowels that go in the 4 external holes of the Torsion Collar (Fig.4) has not been found (the specific detail drawing was not found, it might eventually be recovered by searching among the originals in the archive at JET). However, their effect is probably not relevant, so these holes and dowels are not modeled.

The solver is going to be optimized to run on a 64 bits machine. Before that is completed, in order to start tuning the code on conventional hardware, a simplified mesh (Fig 12 (d)-(f)) with about 13000 elements (requiring 1GB for *L*) was realized. This mesh is quite coarse, in the collar teeth region too, so not precise results were expected. The characteristic of Fig.8 was used for all the magnetic elements.

A first simulation was run considering the same configuration analyzed in the previous section. The data obtained (Table 3 line d), although not very precise due to the coarse mesh used, essentially confirm the results of the 2D analysis. In particular, as shown in Fig 12f, there are only two long brick elements in the vertical direction representing the collar teeth. So the spatial gradient in the *z* direction is not expected to be accurately represented for the very small region occupied by the collar sensors (Fig.6).

To give account of all the involved phenomenon, the model needs to be optimized and, in order to separate the various effects, dry run with zero TF currents will need to be analyzed first.

CONCLUSIONS AND FUTURE WORK

All sensors of the EVP system provide useful signals, which are regularly stored in CODAS and included in the set of JPF files. In particular, six out of the seven probes (namely the six Limb Probes, including in total 18 out of the 22 magnetic sensors) were functionally commissioned and are scientifically exploitable.

Although the measurements provided by the Collar Probe are correct and reliable as well, their use remains questionable, since they are strongly affected by the local geometry of the iron, which is responsible for a considerable gradient of the field. In addition, the reorientation of the magnetic domains in response to the rise of the TF and PF currents produce some remarkable nonlinear 3D effects.

The results of the 2D modeling confirms the qualitative analysis. They were obtained under the following assumptions:

- Considering the time scale of the TF and PF currents, the eddy currents effects were neglected, so that a magnetostatic modeling could be adopted. This assumption calls for a quantitative assessment. For this reason a further phase of the study will include a 3D eddy current model of major massive components of the iron collar. Although it is expected that these effects are not very relevant.

- The same *H-B* curve was used for all magnetic materials. That is actually not important when modeling the JET machine because the central column of the magnetic circuit is nearly always fully saturated, and $H \quad 0$ in the limbs as they are always far from saturation. However, this assumption could be not acceptable when dealing with the prediction of the field value in the vicinity of the iron, in particular in the collar region.

The results of the 3D modeling activity substantially confirm the 2D ones. The method used, which implements an iterative procedure based on an integral formulation, requires an hardware with large amount of RAM memory to be optimised. That will be done in future activities, where a sensitivity analysis (versus permeability descriptions and versus refinement and optimization of the mesh) will be performed, and the effect of eddy currents circulating in the passive structures will be taken into account.

A subsequent activity will be to reimplement the solver using a fast method [41], in order to be able to simulate more accurate models and to reduce the computation time and the hardware requirements.

The detailed 3D analysis can also be used to provide a prediction tool, when wishing to move the collar probes into a different position. This intervention looks attractive in view of a better usability of the Collar Probe.

ACKNOWLEDGEMENTS

This work, supported by the European Communities under the contract of Association EURATOM-ENEA, was carried out within the framework the European Fusion Development Agreement. The views and opinions expressed herein do not necessarily reflect those of the European Commission. The authors are grateful to G Chitarin, V Coccorese and S Peruzzo for suggestions, information and discussion on the JET ex-vessel probes; to G Artaserse, R Baker, J Bird, J Last, M Furno Palumbo, S Gerasimov, C Marren, F Maviglia, A Murari, E Solano and V Thompson for useful discussions; and to R Albanese and G Rubinacci for their valuable hints regarding the 2D and 3D analysis.

REFERENCES

[1]. *JET Ex-Vessel Magnetics – Enhancement Project 2005* http://users.jet.efda.org/pages/mags/jet-ep/ex-vessel- 2005/ex-vessel-2005.html

[2]. *JET-EP-MAG Project documentation: JETNET folder* J:\EP Diagnostic Enhancements\EP1\MAG

[3]. *JET Torus Design and Installation Unit* http://users.jet.efda.org/pages/torus-ops/index.html

[4]. G. Chitarin, G. Artaserse, A. Quercia, S. Gerasimov, *JET EPMAG Enhancement* Project: Intermediate Report on Installation and Commissioning of *the Ex-Vessel Subsystem*, EFDA document EP-DIA-MAG-R-075, Issue 0, JET Laboratories, Culham, UK, 28 Mar 2006

[5]. V. Coccorese, G. Artaserse, G. Chitarin, A. Quercia, A. Murari, S. Gerasimov, *Assessment of new ex-vessel magnetic measurements in JET*, Review of Scientific Instruments **77**, 10E317 (2006)

[6]. V. Coccorese, G. Artaserse, G. Chitarin, T. Edlington, S. Gerasimov, S. Peruzzo, A. Quercia, C. Sowden, *Manufacturing and Commissioning of the new Ex-Vessel Magnetic Diagnostics System for JET*, Fusion Engineering and Design **82** (2007) 1348–1358

[7]. G. Chitarin, F. Basso, V. Coccorese, S. Peruzzo, N. Pomaro, T. Edlington, C. Sowden, S. Cramp, K. Fullard, *Design of ex-vessel magnetic probes for JET-EP*, Fusion Engineering and Design **74** (2005) 727-731

[8]. A. Lioure, A. Kaye, A. Murari, J. Sanchez, T. Todd, C. Damiani, J. Pamela, The JET-Enhanced Performance programme: More heating power and *diagnostic capabilities in preparation for ITER*, Fusion Engineering and Design **74** (2005) 141-146

[9]. A. Quercia, *JET EP2 Magnetic Diagnostics Enhancement, Radiationhard Hall Probes, Review and Status to Date*, EFDA document EP2-RHP-TEC-0nn-20090730-review, JET Laboratories, Culham, UK, 30 July 2009. http://users.jet.efda.org/pages/mags/jet-ep/ep2/ep2- index.html

[10]. G. Chitarin, *List of reliable signals for EVP magnetics, personal communication*, 05.06.2007

[11]. *Octant Sectional Elevation*, JET configuration drawing CON900026, Issue A, 19.01.1994 (The previous version of this drawing, titled *Layout Poloidal Field System*, shows that the P1 solenoid was initially shorter, consisting of 8 coils instead of 10)

[12]. J.R.Last, D. Cacaut, A.P. Pratt, J.C. Rauch, P.J. Ferry, U. Arensmann, A. Alvarez, *Poloidal Coils and Transformer Core for JET – Design and Manufacture*, IEEE Transactions on Magnetics **17** (5), 1923-1926 (Sep 1981)

[13]. G. Chitarin, *JET EP MAG Enhancement Project: Cable Tests for the Collar Probe Commissioning*, EFDA document EP-DIA-MAG-R-078, Issue 1, 11 Dec 2006

[14]. G. Chitarin, *personal communications*, 06.09.2006, 25.10.2006, 11.12.2006 (2 messages), 20.12.2006, 22.12.2006, 08.01.2007, 09.01.2007, 12.02.2007, 05.06.2007, 09.04.2008

[15]. S. Peruzzo, *Minutes of the Progress Meeting on Magnetic Diagnostics Enhancement (06.06.2007)*, EFDA document EP-DIA-MAG-R-081, Issue 1, JET Laboratories, Culham, UK, 21 June 2007

[16]. JET original drawings D510-00-000, D620-00-001, D620-01-000, D620- 02-000, D620-03-000, D730-01-000, D730-01-001 (casting, before machining), FN338-110 to FN338-120 (unpublished)

[17]. A. Quercia, R. Fresa, *Magnetic Diagnostics Enhancement, Analysis and possible recalibration of the EVP subsystem (Collar Probe)*, EFDA document EP-DIA-MAG-R-087-Annex2-Quercia, JET Laboratories, Culham, UK, 8 May 2008

[18]. V. Thompson, *personal communication*, 18 Mar 2008

[19]. P. Noll, *Earthing of JET Components*, UKAEA CODAS document JTS/H(02)768, Issue 3 reviewed by K Fullard, 3 Aug 2002 http://users.jet.efda.org/pages/mags/index.html

[20]. J. Last, *JET Earthing Rules*, UKAEA Culham Division, Chief Engineer document CD/CE/00/G002, Issue 1, Oct 2003 http://users.jet.efda.org/pages/torus-ops/pages/chiefeng/documents/cdce00g002.pdf

[21]. J. Last, *Notes on Earthing the Magnet Structure*, UKAEA Memorandum,28 June 2007 (document without reference number <earthing magnet structure.doc>, personal

communication, 16 Sep 2008)

[22]. J.R. Last, *personal communication*, 11 Apr 2008 <GS 45.3 permeability.pdf>, <GS 45.3 resistivity.pdf>

[23]. M. Huguet, K. Dietz, J L Hemmerich, J.R. Last, The JET machine: Design, *Construction and Operation of the Major Systems*, Fusion Technology **11**, 43-70 (Jan 1987)

[24]. J. Last, *JET Magnet System*, slides, 07 Dec 2001 http://users.jet.efda.org/pages/torus-ops/pages/enganalysis/magnet-system/magnetsystem.ppt

[25]. J.R. Last, E. Bertolini, M. Buzio, J. Jeskins, P. Miele, S. Papastergiou, P. Presle, V. Riccardo, *Analysis and Tests in Support of Upgrading the JET Toroidal Field to 4 Tesla*, Proceeding of the 15th International Conference on Magnet Technology (MT15), October 20–24, 1997

[26]. E. Bertolini, M. Buzio, A. Kaye, J.R. Last, P. Miele, P. Noll, S. Papastergiou, V. Riccardo, G. Sannazzaro, M. Sjoholm, R. Walton, *Raising the JET Toroidal Field to 4 Tesla, A feasability study relating to torus components*, 29 Nov 1999 http://users.jet.efda.org/pages/torus-ops/pages/enganalysis/ tfupgrade.htm

[27]. R. Albanese, *personal communications*, 17 Mar 2008 (2 messages), 20 Jan 2009

[28]. *JET Iron Core Model – Materials and Discussions* http://users.jet.efda.org/pages/mags/jet-model/model3dindex. html

[29]. A.W. Paynter, *Operations' Handbook*, JET internal document, April 1996

[30]. F. Maviglia, R. Albanese, A. Alonso, T. Bellizio, G. De Tommasi, P. Lomas, A. Pironti, A. Quercia, F. Sartori, L. Zabeo, *Status of the ongoing work on the breakdown*, EFDA-JET PCU-2 Technical meeting, 09 June 2009

[31]. Bruce P. Bardes Ed, *Metals Handbook Ninth Ed, Vol 1, Properties and Selection: Irons and Steels*, American Society for Metals, 1978, p 150

[32]. R. Steiner, ASM, *ASM Handbook Volume 1, Properties and Selection: Irons, Steels, and High-Performance Alloys*, American Society for Metals, 10th ed, 1990

[33]. G.W. Carter, *The electromagnetic field in its engineering aspects*, 2nd ed, Longmans, London, 1967

[34]. Online Materials Information Resource, www.matweb.com

[35]. R.B. Ross, *Metallic Materials Specification Handbook*, 3rd edition, E. & F.N. Spon, 1980

[36]. R. Albanese, F.I. Hantila, G. Rubinacci, *A Nonlinear Eddy Current Integral Formulation in Terms of a Two-Component Density Vector Potential*, IEEE Transactions on Magnetics 32, No 3, (May 1996) 784-787

[37]. R. Albanese, G. Rubinacci, *Finite Element Method for the Solution of 3D Eddy Current Problems*, Advances in Images and Electron Physics **102** (1998) 1-86

[38]. R. Albanese, R. Fresa, G. Rubinacci, S. Ventre, F. Villone, *CARIDDI Users* Guide, Eddy Current Models and Procedures for the Electro-Magnetic *Analysis of ITER Components*, EFDA Study Contract 02-699 Part 1, 2004

[39]. *JET PF Coils Model – PF Circuits and Voltages* http://users.jet.efda.org/pages/mags/jet-model/pfcoils/ circuit/circuit.html http://users.jet.efda.org/pages/mags/jet-model/pfcoils/ pf circuit jpf/pf circuit jpf.html

[40]. *JET Magnetic Diagnostics Data Acquisition Systems* – TF compensation of the Magnetics http://users.jet.efda.org/pages/mags/das/das-index.html

[41]. W.C. Chew, J.M. Jin, E. Michielssen, J. Song, *Fast and Efficient Algorithms in Computational Electromagnetics*, Artech House, 2001

Location		Sensor type	#	Measured quantity	Sensor name	Reliable
Limb 3-4	Inner	Pickup	1	B_z	EC31V	Yes
		Hall	2	B_z	EH31V	Yes
		Flux loop	3	$\langle B_z \rangle$	EFL31	Yes
	Centre	Pickup	4	B_z	EC32V	Yes
		Hall	5	B_z	EH32V	Yes
		Flux loop	6	$\langle B_z \rangle$	EFL32	Yes
	Outer	Pickup	7	B_z	EC33V	Yes
		Hall	8	B_z	EH33V	Yes
		Flux loop	9	$\langle B_z \rangle$	EFL33	Yes
Limb 8-1	Inner	Pickup	10	B_z	EC81V	Yes
		Hall	11	B_z	EH81V	Yes
		Flux loop	12	$\langle B_z \rangle$	EFL81	Yes
	Centre	Pickup	13	B_z	EC82V	Yes
		Hall	14	B_z	EH82V	Yes
		Flux loop	15	$\langle B_z \rangle$	EFL82	Yes
	Outer	Pickup	16	B_z	EC83V	Yes
		Hall	17	B_z	EH83V	Yes
		Flux loop	18	$\langle B_z \rangle$	EFL83	Yes
Collar Octant 4		Pickup	19	$\langle B_z \rangle$	ECC4R	Yes
		Hall	20	B_r	EHC4R	Yes
		Pickup	21	$\langle B_z \rangle$	ECC4V	Yes
		Hall	20	B_z	EHC4V	Yes
		Pt1000	20	Temperature	EC4<TMP	Yes

Timing informations:

JPF Type	Sampling Frequency	JPF Node	URL (example)
DPF	5 kHz (switchable to 10 kHz)	DA/CDE- (sensor name)	JPF/64444/DA/CDE-EC31V
JPF	500 Hz	DA/C2E- (sensor name)	JPF/64444/DA/C2E-EC31V
QPF	100 Hz	DA/CQE- (sensor name)	JPF/64444/DA/CQE-EC31V

Table 1: The JPF chennels produced by the EVP system. The signals are recorded by the CODAS KC1E data acquisition system, at 3 frequencies between either PRE (Start Pre-pulse Action) or SJP (Start JET Pulse) and EJP (End of JET Pulse). Notice that, due to the presence of a significant spatial gradient in the collar region, the measures performed by the pickup coils in the Collar Probe have to be identified as spatial averages, and not as as local values.

Magnetic Circuit
P1 Coil Support Rings: high-resistance, 13% Cr Steel
Limbs and Centre Pieces: low impurity steel, Nomatil RD 0.65 mm thick laminations insulated with an organic varnish
Centre Pillar: low impurity steel, Nomatil RD Radial sectors of laminations enclosed in an epoxy glass tube and vacuum impregnated with epoxy resin
Mechanical Structure / Magnetic Circuit
Torsion Collar: GS 45 3 DIN 1681
Collar Teeth: 38 Ni Cr Mo 4 Low Carbon Alloy Steel Fe 96% , C 0.38% , Ni 1% , Cr 0.80% , Mo 0.25% $\mu_0 M_{sat} \cong 2{:}11$ T, $\mu_{r;max} \cong 2000$, $H_{coerc} \cong 150$ A/m
Collar shear dowels: C30
Inner Cylinder: Stainless Steel ASTM A240 Tip 304
Inner Cylinder Dowel: Carbon Steel ASTM A434 Class BB
Shell (mechanical structure) and Rings (& Ring Teeth): Austenitic Cast Iron with spheroidal graphite GGG Ni Mn 13 7
Shell shear dowels: C30
Shear Keys (between shell octants): AISI 304N

Table 2: Materials for the JET magnetic circuit [12, 22] and the mechanical structure. The Torsion Collars (and the Collar Teeth) are the only components of the mechanical structure made of ferritic steel because they are also used as part of the magnetic circuit [23].

		Hall Sensors		Pick-up coils		difference Hall − Coil	
		EHC4R	ECC4V	EHC4R	ECC4V		
		B_r [mT]	B_z [mT]	B_r [mT]	B_z [mT]	ΔB_r %	DB_z %
a	2D Simulation Smooth Torsion Collar	−80.4	158	− 81.6	157	−1	1
b	2D Simulation Torsion Collar with axisymmetric tooth	− 123	65.6	−149	64.9	−17	1
c	2D Simulation Torsion Collar with axisymmetric tooth and through hole	− 121	78.1	−144	61.3	−16	27
d	3D Simulation (coarse mesh) Torsion Collar with 3D tooth and through hole	− 117	91.8	−143	92.1	−18	~ 0
e	Experimental values with linear TF compensation (and polarity correction, see before)	− 211	95.8	−168	123	26	− 22
		EHC4R	ECC4V	EHC4R	ECC4V	differences among the simulations	
		ΔB_r %	ΔB_z %	ΔB_r %	ΔB_z %		
b – a	(values case b) – (values case a)	53	− 58	82	− 59		
c – b	(values case c) – (values case b)	− 2	19	− 4	−5		

Table 3: Result and comparisons of the magnetostatic simulations and the experimental values for the sensors in the Upper Collar region at t = *48.5s of the standard dry run Pulse No: 64444. Line d shows the preliminary outcome of the 3D modelling activities.*

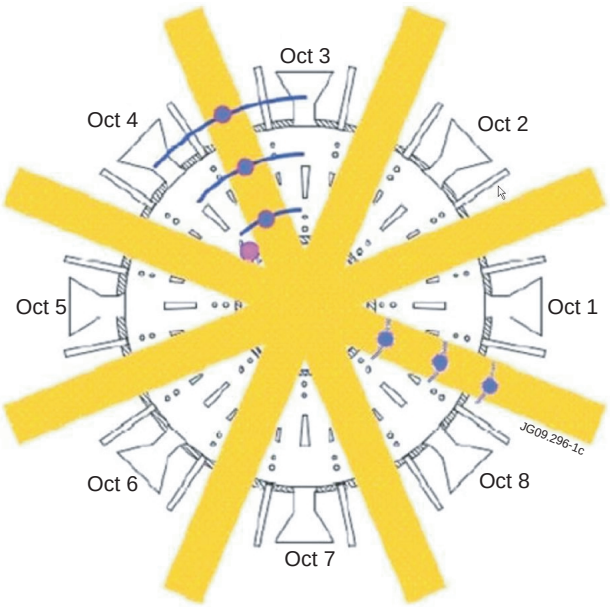

Figure 1: Schematic top view of the JET machine, showing the Ex-Vessel magnetic diagnostic system. The blue dots show the location of both the pickup coils and the Hall sensors, the blue arcs depict the (local) flux-loops and the purple dot represents the collar probe.

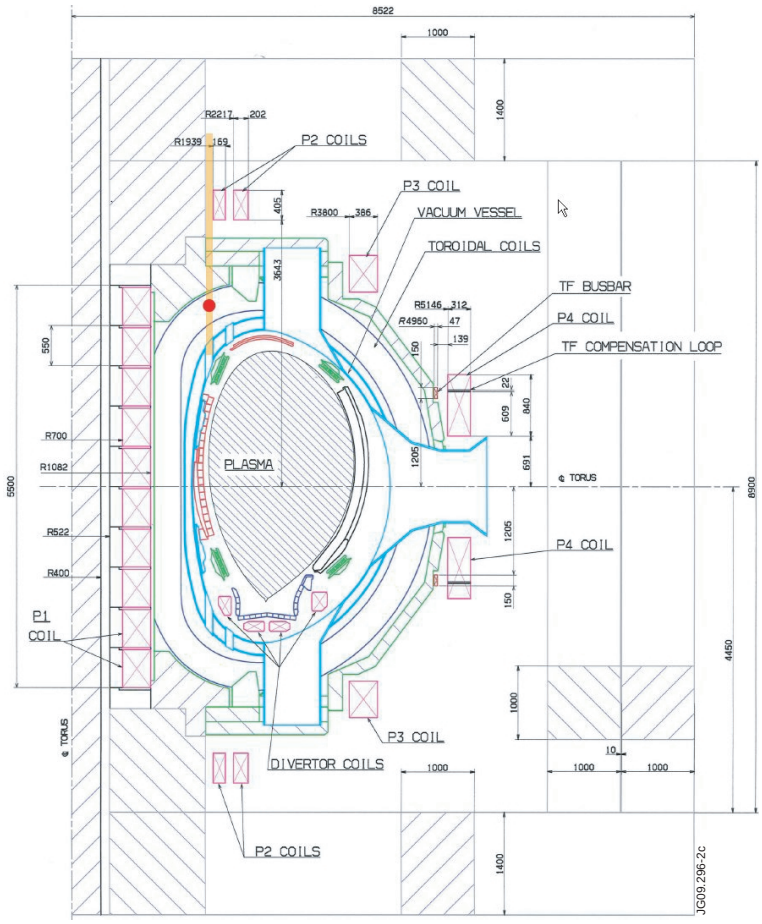

Figure 2: Cross-section configuration of the JET machine (19.01.1994) [11]. The red dot schematically represents the location of the Collar Probe. The (upper and lower) collar teeth, described later, are not shown here. The P1 solenoid consists of 10 coils: originally it was shorter (consisted of 8 coils) [12].

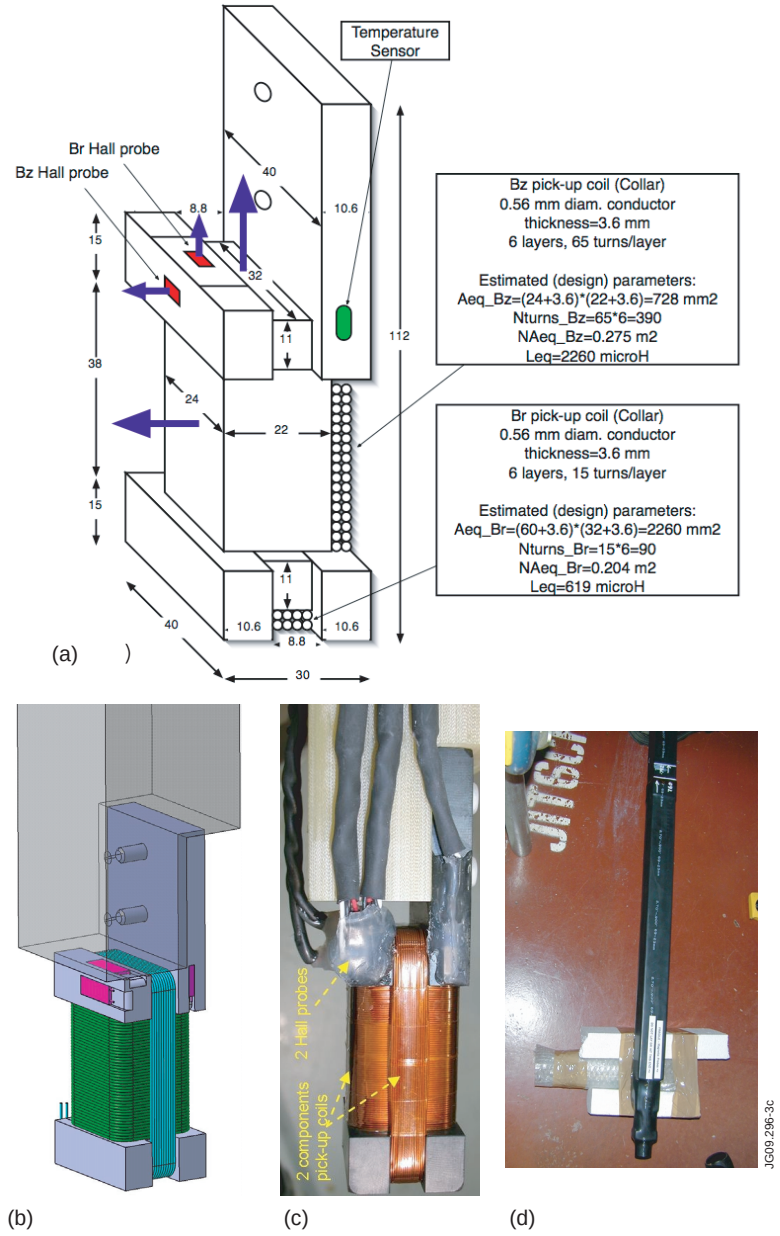

Figure 3: Collar Probe. (a) Model of the insulating former for the B_r and B_z pick-up coils and Hall sensors; the temperature sensor is also shown. The principal parameters of the coils are indicated in the boxes. (b) CAD model. (c) The probe. (d) The probe mounted on its dielectric supporting bar, before installation.

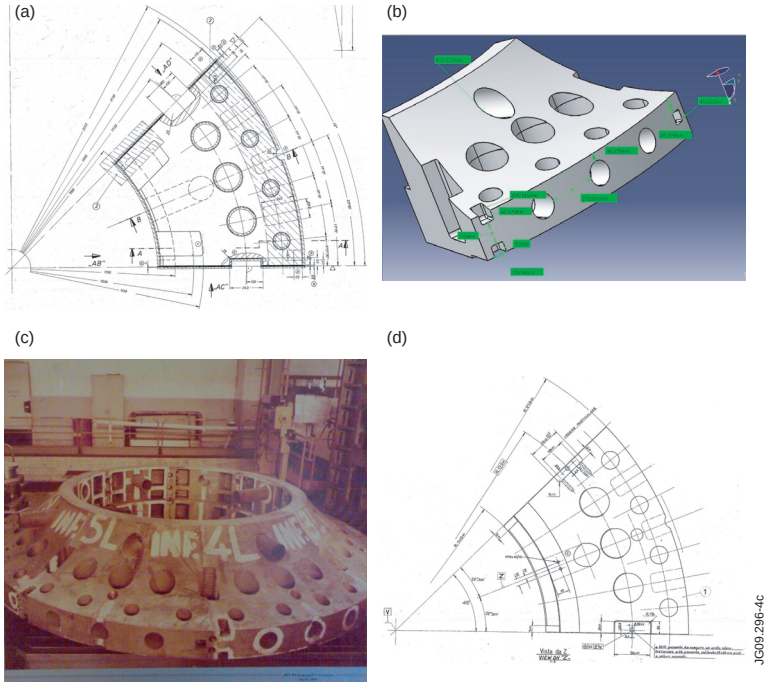

Figure 4: The Torsion Collar. (a) Particular from the original JET casting drawing D730-01-001 of the torsion collar component, where a smaller central through hole is missing, because it appears after machining. (b) CAD model of the torsion collar. (c) Picture of the complete torsion collar, taken during the construction phase of JET; the mentioned smaller hole is present. (d) Particular from the original JET assembly drawing D730-01-000 of the upper collar; the smaller central hole next to the larger central one is visible.

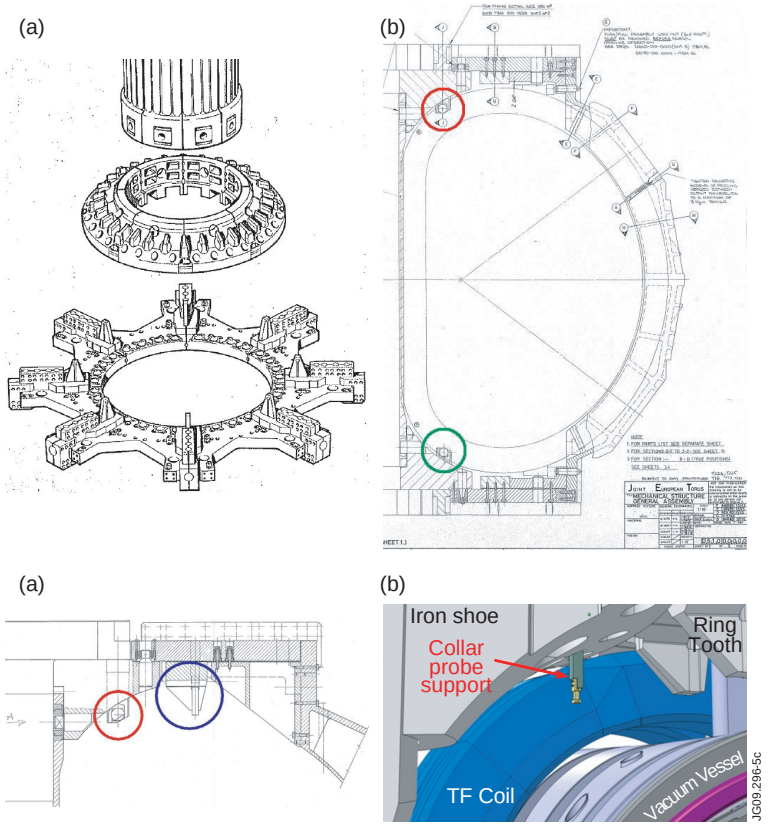

Figure 5: (a,b) Illustration of selected parts of the JET mechanical structure. (c,d) Particular and CAD model

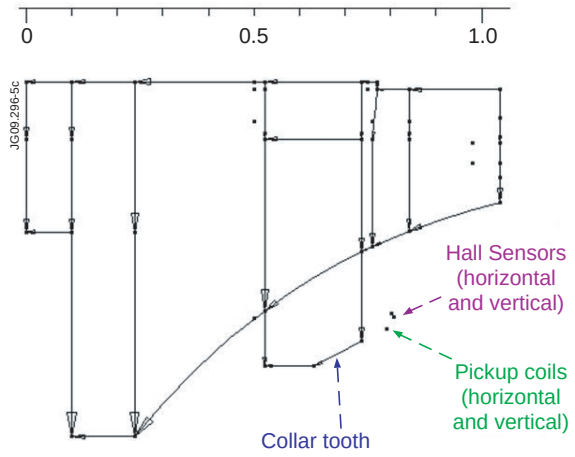

Figure 6: Representation of the relevant poloidal section in the collar region. The 'toroidal thickness' of the teeth extends over 3 degrees.

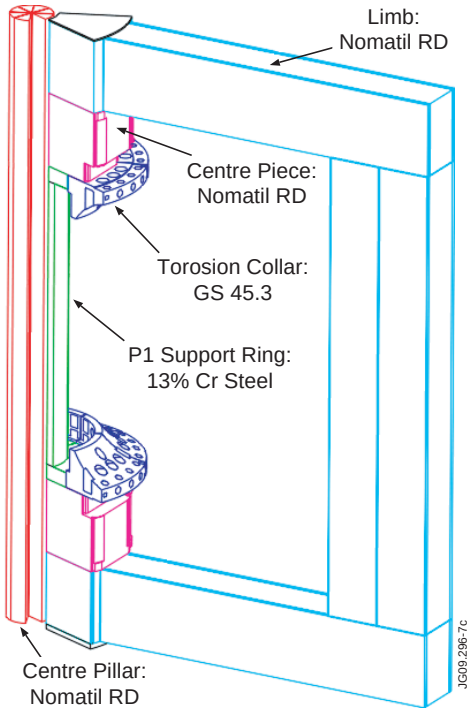

Figure 7: Materials of the JETmagnetic circuit. The Collar Teeth are not shown.

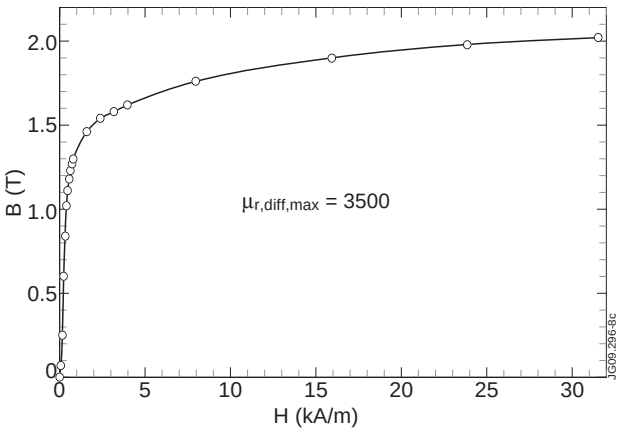

Figure 8: Part of the non-hysteretic H-B characteristic used in most JET simulators. The maximum value of the differential relative permeability $\mu_{r,diff} = 1/\mu_0\ dB/dH$ is indicated. The saturated part of the curve is not shown, the lookup table contains more data, and values extrapolated to $dB/dH = \mu_0$ as well, up to tenths of Tesla.

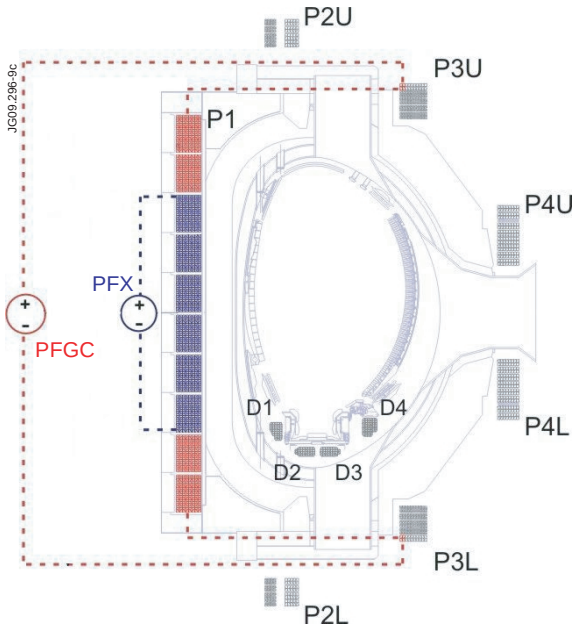

Figure 9: Primary (red dashed line) and PFX (blue dashed line) circuits. A typical JPF node for the current IPRIM flowing in the primary circuit is PF/SC-IP1<MS. That is sometimes a little confusing, because I_{PRIM} isn't just the current in the P1 coil. In particular, 4 turns of the P3 coils (2 in the P3U and 2 in the P3L) also belong to the primary circuit. The current in the six coils of the P1 solenoid depicted in blue is $I_{PRIM} + I_{PFX}$.

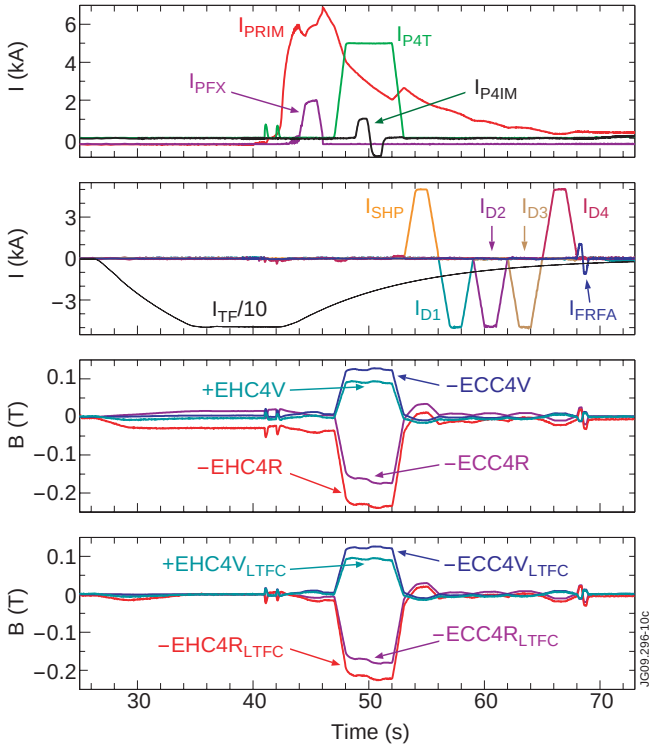

Figure 10: Waveforms for the JET standard dry run Pulse No: 64444. The experimental signals produced by the magnetic sensors (last two plots) have been corrected for the polarity. That is not necessary for more recent pulses, because the right polarity changes were applied to the data acquisition chain.

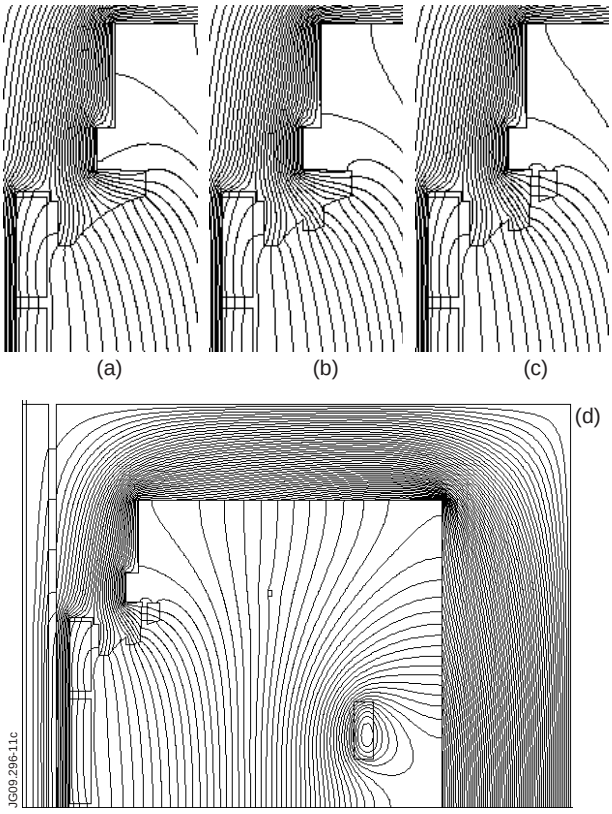

Figure 11: Axisymmetic flux maps for standard dry run Pulse No: 64444 at t = 48.5s. Only I_{PRIM}, I_{P4T} and TF currents are nonzero.

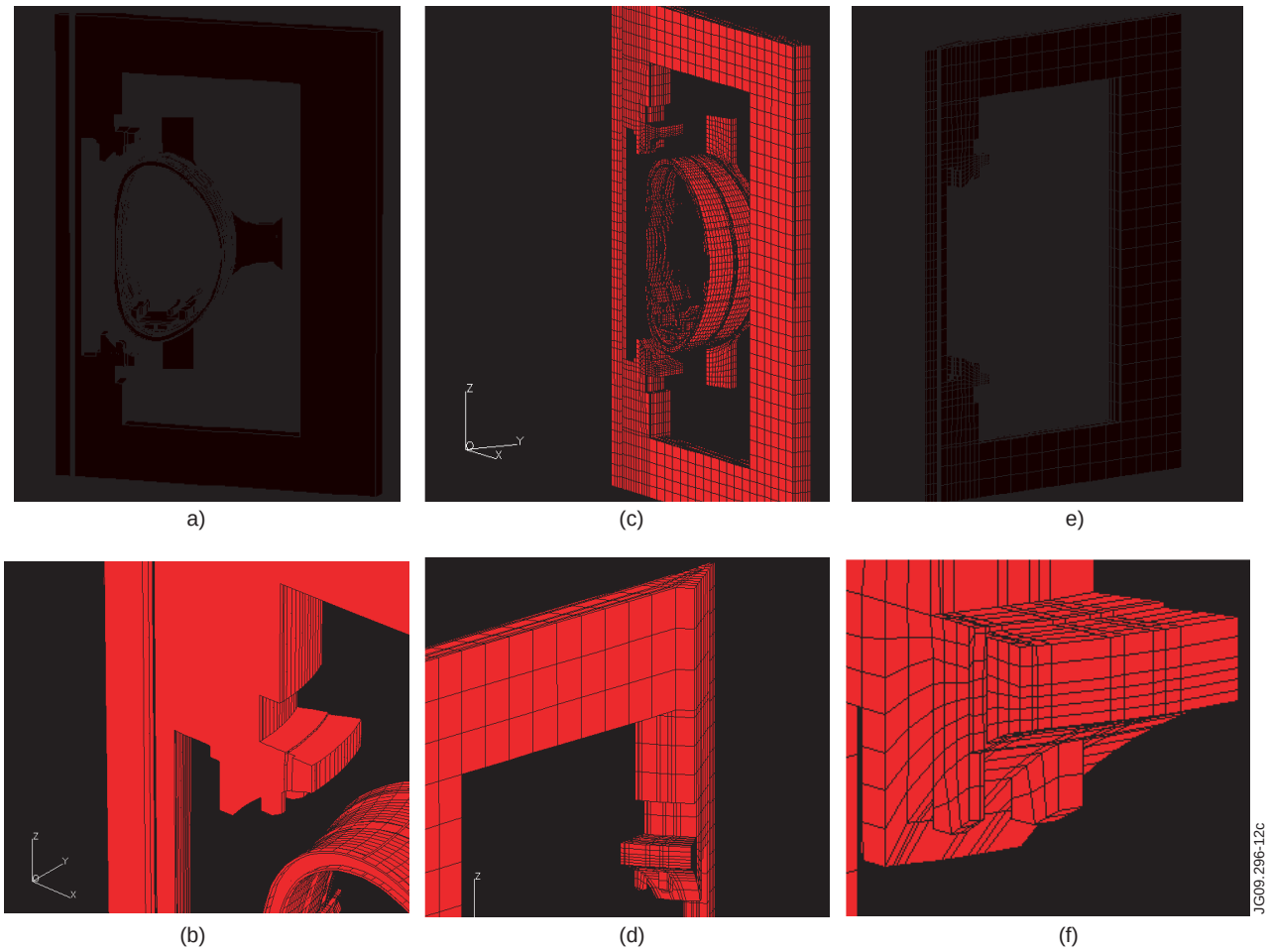

Figure 12: 3D model integrated with the CARIDDI solver. (a)-(c) Grid consisting of 26052 brick elements, 42963 nodes and 94687 faces. (d)-(f) Coarse grid with about 13000 brick elements (4426 elements for the magnetic circuit only).